Microwave Modeling of 2-D Active Grid Antenna Arrays

Aleksandar Pance, *Student Member, IEEE,* and Michael J. Wengler, *Member, IEEE*

Abstract—**We present a new measurement technique for determining the broadband driving point impedance of large two-dimensional active grid arrays. The active array radiates a plane wave in the broadside direction when all elements are locked in phase. For analysis, the array is reduced to a single unit cell by exploiting the array symmetries. We determine the driving point impedance of the unit cell by using the Dielectric Waveguide Measurement method (DWM). The approximations of the method are discussed and the method is compared with other measurement techniques. We present results for four square arrays: dipole, bow-tie, double-Vee and slot array. We verify our measurement method by comparing it to the full-wave theory in the whole range. We show that the results for the dipole and the bow-tie arrays agree very well with the quasistatic theory and the results of others. We extend the quasistatic theory to the doube-Vee array with excellent agreement and present a modified quasistatic circuit for the slot array. Finally, we show that all four antenna arrays can be represented by very simple circuits that use only transmission lines as circuit elements. We find that the bow-tie array represents the best choice for broadband operation.**

I. Introduction

IN RECENT years there has been a growing need for power sources in the millimeter and submillimeter frequency range. Solid state oscillators are limited by low power levels. Conventional high power tubes are expensive, bulky, inefficient and inconvenient. It has recently been demonstrated that sources with sufficient power levels in the microwave and millimeter range can be accomplished by quasioptical power combining of a large number of low power solid state sources [1]–[3]. We are investigating active grid arrays for the submillimeter frequency range [4], [5].

The active grid array is a large 2-D array of "active antennas". Each "active antenna" consists of a solid state oscillator integrated with a short antenna. The power radiated from each "active antenna" is quasioptically combined to give useful power levels.

In order to design an array for maximum radiated power, we need to know the driving point impedance presented by the array at the leads of each active device. This paper describes measurements of that impedance using microwave scale models. The paper is organized as follows. In Section II we present important properties of 2-D active antenna arrays. Section III describes measurements using 2-D and 0-D microwave models. In Section IV we present a new measurement technique based on the 0-D microwave model of the array. We discuss its approximations and limitations. In Section V we present the results of our measurement technique for four arrays of interest: dipole, bow-tie, double-Vee and slot.

Manuscript received Aug. 20, 1991; revised Apr. 21, 1992. This work was supported by the Air Force Office of Scientific Research grant AFOSR-90-0233. A. Pance was supported by the Link Energy Foundation Fellowship.

The authors are with the Department of Electrical Engineering, University of Rochester, Rochester, NY 14627.

IEEE Log Number 9204034.

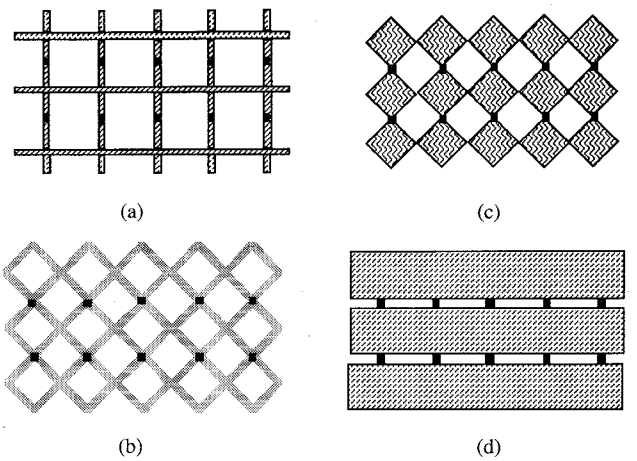

Fig. 1. 2-D antenna arrays: (a) Dipole array. (b) Bow-tie array. (c) Double-Vee array. (d) Slot array.

II. 2-D Active Antenna Arrays

We are interested in planar antenna arrays on dielectric substrates that are fabricated using standard photolithographic techniques. We focus our attention on four different rectangular arrays: dipole array, bow-tie array, double-Vee array and slot array (Fig. 1). However, the discussion that follows is in no way limited to these four geometries.

In the desired mode of operation, all antennas are driven with equal amplitude and phase. The array radiates a plane wave in the broadside direction, both to free space in front of the array and to the substrate behind it. Usually, a reflector is placed behind the array to provide a feedback signal for phase-locking of the individual oscillators.

Baseband Operation

Because of its periodic regularities, an array will have resonances at wavelengths which are close to integer multiples of the grid spacing. We describe these resonances below in Section IV. An array designed for operation at one of these resonances would operate over much less than one octave. A design for operation between the first and second resonances of the array might yield close to one octave of performance. We are interested in arrays operated over a very broad band, a

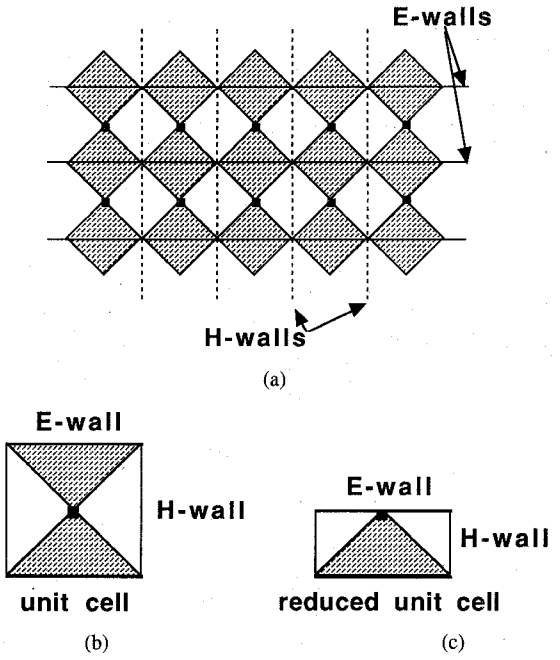

Fig. 2. (a) Locations of symmetry planes determine magnetic and electric walls in infinite 2-D array. (b) The cross-section of the equivalent 0-D array. The unit cell consists of a single antenna in a waveguide with electric walls top and bottom and magnetic walls at the sides. (c) The reduced unit cell constructed using the horizontal symmetry plane of the unit cell.

few octaves at least. An array designed for operation between its zeroth resonance (dc) and its first resonance fulfills this goal. We refer to this kind of design as a "baseband" design.

Baseband arrays can be analyzed in a quasistatic way. A quasistatic equivalent circuit of the array should certainly be accurate at very low frequencies. As we will see below, we do in fact find quasistatic equivalent circuits for the arrays we measure which are accurate from dc up to the first resonance of the array.

Array Symmetries

Fig. 2(a) shows a number of horizontal and vertical symmetry planes of the rectangular array. When every element of the array is oscillating with equal phase and amplitude, horizontal symmetry planes have the properties of electric walls, and vertical symmetry planes are like magnetic walls.

An equivalent 0-D array is constructed by "cutting" the array along two electric and two magnetic walls. The unit cell (Fig. 2(b)) consists of a single antenna in a waveguide with electric walls top and bottom and magnetic walls at the sides. The waveguide is filled with the dielectric behind the antenna and is empty in front of it. We will refer to this waveguide as the "ideal waveguide." The unit cell itself has two additional planes of symmetry: a horizontal electric wall and a vertical magnetic wall. For reasons that we will explain later, we utilize only the electric wall to define a reduced unit cell (Fig. 2(c)) which is used in microwave measurements.

Transmission Line Model

In the baseband operation mode, the array can be represented by the simple transmission line model (Fig. 3): a two

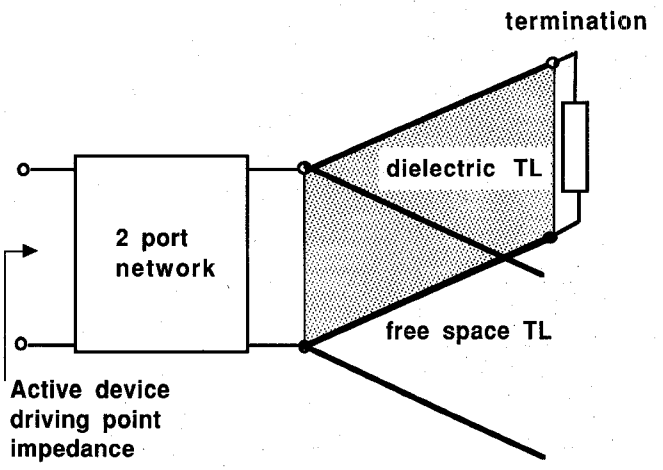

Fig. 3. Transmission line model of the 2-D array based on the unit cell. Dielectric and free space transmission lines stand for the dielectric-filled and empty parts of the waveguide, respectively.

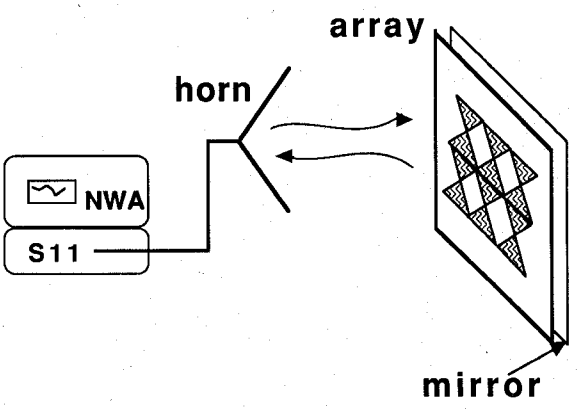

Fig. 4. Driving point impedance measurement of Lam *et al.* [7].

port network feeding dielectric and free-space transmission lines that correspond to the dielectric-filled and empty parts of the waveguide, respectively [6]. Since baseband operation mode covers the "long wavelength" limit, the equivalent circuit of the two-port network can be found from a quasistatic approximation.

III. Microwave Models of the Array

The equivalent circuit of the two-port network representing the antenna array is determined from measurements of the driving point impedance on microwave scale models.

2-D Model

Lam *et al.* [7] determine the driving point impedance by measuring a 2-D scale model of the array. The measurement is performed as follows: the vector network analyzer feeds the horn antenna that illuminates the 2-D model (Fig. 4). All ports of the model are shorted or opened and the reflection coefficient is measured. The driving point impedance is determined by fitting the measurement to candidate equivalent circuits. The effects of the horn antenna need to be deembedded from the measurement.

0-D Model

We have devised the measurement technique based on the model of the 0-D equivalent array, described earlier. We call this measurement technique the Dielectric Waveguide Measurement (DWM) method. Measurements are performed on the reduced unit cell (Fig. 2). The reduced unit cell is chosen because the measurement port is directly accessible from the top wall of the waveguide, so the measurement probe doesn't perturb the antenna near field. The active element in the reduced unit cell is driving only one half of the antenna, so the measured driving point impedance is half the impedance of the full unit cell. The magnetic walls at the sides of the reduced unit cell are approximated by the dielectric-air boundary. Note that the inverse approximation (dielectric-air boundary approximated as a magnetic wall) is used extensively, e.g., in calculations of the modes of dielectric resonators [8].

IV. Dielectric Waveguide Measurement (DWM) Method

DWM Setup: The "Desktop Antenna Range"

Our measurement setup (Fig. 5) is a realization of the reduced unit cell (Fig. 2(c)). It consists of a 120 cm long rectangular parallel plate transmission line, partially occupied by a rectangular dielectric rod of the same cross-section (2.54 cm wide and 1.27 cm high). Parallel metal plates form the top and bottom walls of the reduced unit cell. The antenna is modeled with copper tape at the boundary between the dielectric part and the free space part of the transmission line. The antenna is contacted with an SMA connector through a small hole in the upper plate. The dielectric used is "Stycast HiK" with $\epsilon_r = 12$ from Emerson & Cuming, Inc. The dielectric side of the transmission line is terminated with a short circuit, and the free space side with microwave absorber.

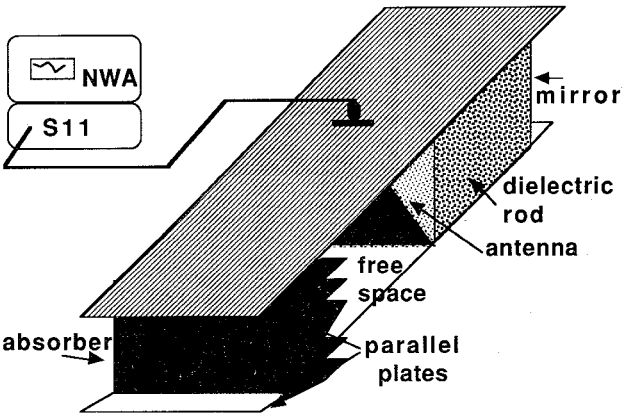

Fig. 5. DWM method setup: The "desktop antenna range." Parallel metal plates form the free space transmission line (92.6 cm long) on one side of the antenna and the dielectric transmission line (27.6 cm long) with the dielectric rod ($\epsilon_r = 12$) on the other side. Free space side is terminated with an absorber and the dielectric side with the contacting short circuit. The dimensions of the cross-section are 2.54 cm × 1.27 cm. Antenna port is connected to the HP8720B Vector Network Analyzer.

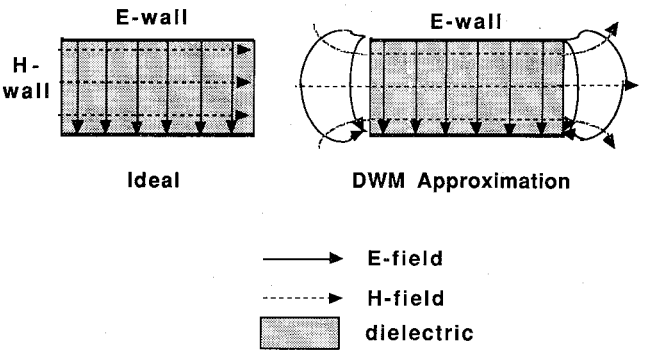

Fig. 6. Field distribution in the ideal waveguide of the reduced unit cell and the DWM model.

Discussion of the DWM Approximation

The approximations used in the DWM method are as follows. The ideal waveguide of the reduced unit cell is approximated by a Dielectric Rod Parallel Plate Transmission Line (DRPPTL) on the dielectric side, and by a Free Space Parallel Plate Transmission Line (FSPPTL) on the free space side. The magnitude of errors in the approximation is reflected in the different characteristic impedances of the transmission lines and somewhat different modes.

The approximation of the magnetic wall with the dielectric-air interface will result in some radiation leakage at the sides, which is confirmed below in our results. The radiation leakage would be smaller for reduced unit cell with smaller aspect ratio (heigh/width), but this is determined by the array geometry. By showing that our approximation works well for square arrays, we are confident that the DWM method is valid for arrays with reduced unit cell aspect ratio ≤ 0.5.

The DRPPTL is a modified dielectric rod waveguide with metal at the top and bottom surfaces. Although the geometry of the DRPPTL is simple, we were unable to find any report on its analysis in the extensive literature about dielectric waveguides (e.g., [9], [10] and related references). However, some insight into the DRPPTL can be gained by considering the H-guide [11].

Modes

Propagating Mode: We want the fields inside the waveguides of our model to be as close as possible to the plane-wave TEM mode of the ideal waveguide. The FSPPTL supports a TEM mode. Because of fringing fields, this TEM mode is not a plane wave. Therefore, the FSPPTL has a lower characteristic impedance than ideal transmission line.

Simple analysis, similar to that in [12], shows that the DRPPTL can not support the pure TE, TM or TEM mode; all modes are hybrid. However, the lowest order mode doesn't have a cutoff frequency and is, as in the case of microstrip, a quasi-TEM mode. For low frequencies, the electric field of this mode is similar to the dc solution for the equivalent capacitor. Therefore, for high dielectric constant, the field distribution inside the DRPPTL is nearly identical to the plane wave of the ideal transmission line (Fig. 6).

Higher Order Modes: Since the reduced unit cell consists of the dielectric and the free space part of the waveguide, the first higher order mode to start propagating will appear in

the dielectric part. Propagation of higher order modes in the 0-D waveguide corresponds to the presence of grating lobes in the 2-D array. The cutoff frequencies of the higher order modes (j,k) in the dielectric side of the ideal reduced cell waveguide are:

$$f_{Cjk} = \frac{c}{4h\sqrt{\epsilon_r}}\sqrt{j^2+4k^2} \tag{1}$$

where c is the free space speed of light, ϵ_r is the dielectric constant, h is the height of the waveguide and j and k are nonnegative integers, different from zero if equal. The cutoff frequencies of the DRPPTL we use to model the ideal waveguide are somewhat lower than this. For frequencies below $f_{C10}(1)$, all higher order modes are evanescent. Coupling to the evanescent modes determines the reactive part of the antenna impedance.

We do not know exactly how the approximation to a magnetic wall affects the evanescent modes. However, as we show below, our measurements agree very well in the whole baseband with calculations based on the full wave analysis, as well as with measurements of other groups. This fact gives us the confidence that the DRPPTL approximates the ideal transmission line well enough for our purpose.

Characteristic Impedance

For the ideal waveguide of the reduced unit cell, the characteristic impedance is given by

$$Z_c = \frac{Z_0}{g\sqrt{\epsilon_r}} \tag{2}$$

where $Z_0 = 377\,\Omega$ and g = width/height. Because of the fringing fields, the characteristic impedance of the FSPPTL is lower than this value, and is calculated by Wheeler [13] using the conformal mapping method (Table I).

The characteristic impedance of the DRPPTL can be estimated using simple arguments. Starting from the parallel plate transmission line completely immersed in the dielectric (Fig. 7a), the characteristic impedance increases as parts of the dielectric are replaced by the free space. This is because the capacitance per unit length decreases. Wheeler [14] calculates the impedance of a parallel plate transmission line separated by an infinite dielectric sheet (Fig. 7(b)). We use his calculation as a lower bound on the impedance of the DRPPTL. The upper bound for the characteristic impedance of the DRPPTL is given by eq. 2 (Fig. 7(d)), which is the value for the ideal waveguide we hope to approximate.

We have measured the characteristic impedance of both the FSPPTL and the DRPPTL with the HP8720B Vector Network Analyzer using different lengths of transmission lines and different terminations, and fitting the measurements to the ideal transmission line. Table I compares the results of our measurements with the lower and upper bounds of the characteristic impedance for several dielectrics. We use these measured values later for the equivalent circuits of the arrays.

TABLE I
CHARACTERISTIC IMPEDANCE OF THE DRPPTL

ϵ_r	Lower Limit [Ω]	Upper Limit [Ω]	Measured [Ω]
30	24.1	34.4	29.2
12	37.7	54.4	40
4	63.7	94.25	80.8
1	116.2	188.5	108

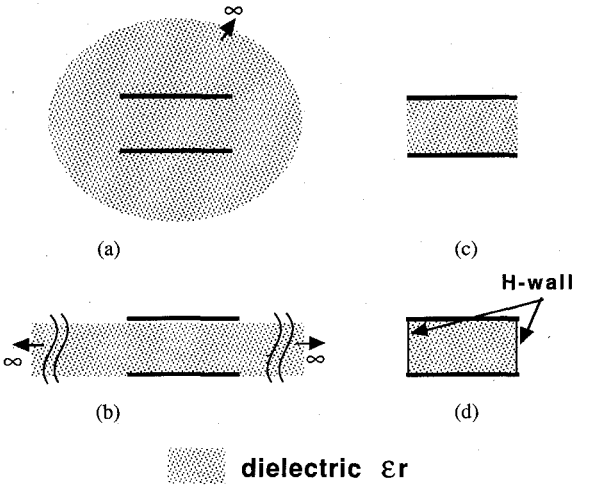

Fig. 7. Cross-sections of several dielectric parallel plate transmission lines in the order of increasing characteristic impedance: (a) Parallel plate transmission line completely enclosed by dielectric medium. (b) Parallel plate transmission line separated by infinite dielectric sheet [14]. (c) Dielectric Rod Parallel Plate Transmission Line (DRPPTL) and (d) ideal transmission line.

Upper Frequency Limits

In our measurement setup, all higher order modes will be evanescent below the frequency f_{hom}:

$$f_{hom}[\text{GHz}] = \frac{7.5}{h\sqrt{\epsilon_r}} \tag{3a}$$

where h is height of the waveguide (in cm). This frequency limit corresponds to the appearance of the substrate modes of the 2-D array. The second limit is given by the resonance of the antenna at the dielectric boundary:

$$f_{ar}[\text{GHz}] = \frac{7.5}{l_r\sqrt{\dfrac{1+\epsilon_r}{2}}} \tag{3b}$$

where l_r is the resonant antenna length (in cm). This is the upper limit for the baseband operation mode. We will discuss these limits in the section on results.

Measurement Procedure

The antenna in the measurement setup is connected to the HP8720B Vector Network Analyzer. The driving point impedance is readily obtained from the measurement of the reflection coefficient. The lowest frequency of the network analyzer is 130 MHz.

We perform two measurements: the "direct" measurement and the "gating" measurement. In the "direct" measurement the DRPPTL is terminated with a short-circuit and the FSPPTL

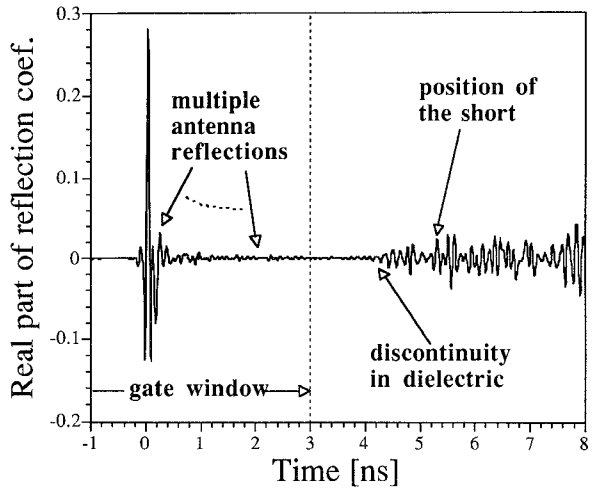

Fig. 8. Time domain bandpass transformation of the reflection coefficient measurement, showing the location of the 6 ns wide gate window.

is "matched" with microwave absorber. In the "gating" measurement, the measurement is performed with both ends of the transmission line matched. Perfectly matched transmission lines are simulated by utilizing the time-domain gating function of the network analyzer. The equivalent circuit of the antenna is extracted from the "gating" measurement. The result of the "direct" measurement is used to verify the equivalent circuit once it has been found.

Using the Time-Domain Gating Function

The gating function [15] is used to remove mathematically reflections from the ends of transmission lines. The span of the gate window needs to be chosen sufficiently wide to include multiple reflections from the ends of the antenna, but sufficiently short to eliminate reflections from the ends of the transmission line. For the dielectric with $\epsilon_r = 12$, the pulse scattered from the end of the antenna will be received at the driving point in 200 ps, while scattering from the end of DRPPTL takes about 5.5 ns (Fig. 8). We have used the 6 ns gate span centered at 0 s to position the end of the gate window about half way to the DRPPTL end.

The equivalent circuit for the matched transmission lines is obtained by fitting the model to the measured data using the "Touchstone" simulation program [16]. The values used in equivalent circuits for the characteristic impedances of the dielectric and free space transmission lines are the measured values shown in Table I. These are doubled in the equivalent circuits because measurements are performed on a model of the reduced unit cell. We always start with a one element equivalent circuit, and we increase the number of elements until a circuit with good fit is obtained. The fit is optimized to reduce the least-squares difference between measurements and equivalent circuit reflection coefficients.

V. Results

We have measured antenna arrays of Fig. 1 using the DWM method. For the measurements with the $\epsilon_r = 12$ dielectric, the f_{hom} frequency limit (3a) is about 1.7 GHz. The antenna resonances, f_{ar}, range from 1.9 GHz for the double-Vee array, to 2.5 GHz for the dipole and bow-tie arrays, and around 3.5 GHz for the slot array.

Dipole Array

According to the quasistatic approximation [7], the dipole array (Fig. 1(a)) is represented by an inductor of the antenna leads feeding the free space and dielectric transmission lines. The capacitance of the horizontal biasing lines can be neglected if the lines are not very wide. The value of the inductance is [7]:

$$L = \frac{\mu_0 h}{2\pi} \ln\left[\csc\left(\frac{\pi w}{2a}\right)\right] \tag{4}$$

where 'h' is the height of the unit cell, 'a' is it's width, 'w' is the width of the dipole and μ_0 is the magnetic permeability of free space.

Fig. 9(a) shows the real and imaginary part of the driving point impedance for the measured data (solid line), and the simple inductance model (dashed line). Excellent agreement is obtained in the frequency range from 200 MHz to 1.5 GHz with the least-squares error of 0.2%. The value of inductance obtained from our measurement, 16.6 nH is within 15% of the quasistatic approximation 14.2 nH. Our results are consistent with those of Lam *et al.* [7] and Weikle [17] for this array. Our equivalent circuit (Fig. 9(b)) has a resistor $R_s = 432\,\Omega$ in parallel with the inductance L. The resistor accounts for the power lost in radiating modes [10] through the dielectric-air boundary. If there was an ideal magnetic wall instead of a dielectric-air boundary, no power would leak out and R_s would be infinite.

Transmission Line Representation

We have found that the simple transmission line (Fig. 10) is a model for the dipole array over a broader frequency range than the lumped component model. The driving point impedance of this model is shown in Fig. 9(a) with dotted lines. Excellent fit is obtained up to 2.3 GHz. The value obtained for the characteristic impedance of the transmission line is $Z_c = 166\,\Omega$. Its length is one-quarter of a wavelength at 2.52 GHz. This value is close to 2.3 GHz, f_{ar} calculated for this antenna. The transmission line equivalent circuit of the dipole allows it to be related meaningfully to the other antenna arrays.

Bow-Tie Array

The results for the bow-tie array of Fig. 1(b) are presented in Fig. 11. The Smith chart is normalized to $100\,\Omega$. The equivalent circuit that gives the best fit is a short transmission line (Fig. 10). We were able to fit this model to the measured data in the range 200 MHz–2.5 GHz, with less than 0.2% error.

The equivalent circuit obtained agrees well with the theoretical predictions and measurements reported in [17], [18]. The characteristic impedance of the short transmission line should be the quasistatic impedance of the bow-tie antenna of the

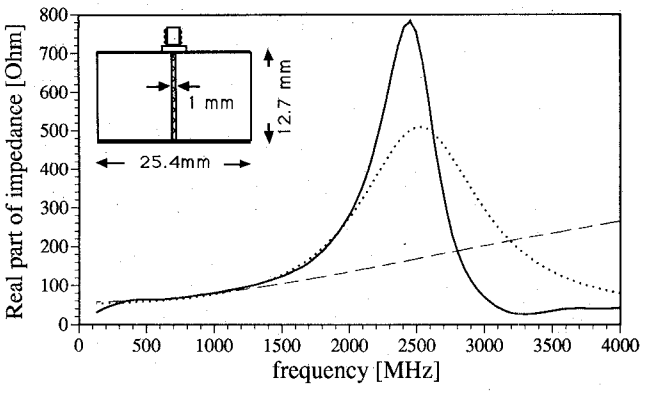

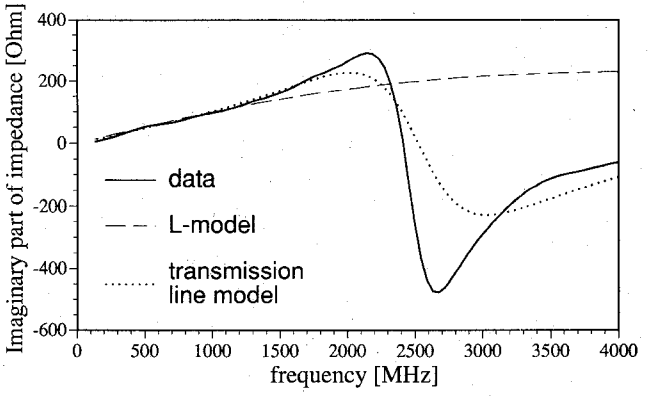

(a)

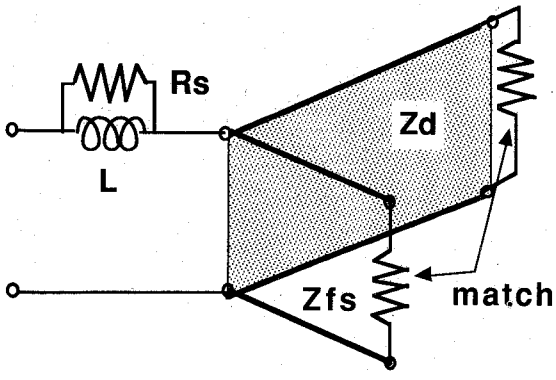

(b)

Fig. 9. Dipole array results. (a) Real and imaginary part of the driving point impedance for the measurement (solid line), simple inductance model (dashed line) and the transmission line model (dotted line). (b) Inductance model: L = 16.6 nH, $R_s = 432\,\Omega$, the dielectric $Z_d = 78.4\,\Omega$ and the free space $Z_{fs} = 216\,\Omega$ transmission lines. The resistance is an artifact of the measurement technique due to radiation losses.

given geometry [19]:

$$Z_{bt} = \frac{Z_0}{\sqrt{\frac{1+\epsilon_r}{2}}}\frac{K(k)}{K'(k)}, \qquad k = \tan^2\left(45^\circ - \frac{\theta}{4}\right) \tag{5}$$

where Z_0 is the free space impedance, ϵ_r is the dielectric constant, $K(k)$ is the complete elliptic integral of the first kind, $K'(k) = K(1-k^2)$ and θ is the angle of the bow-tie. In our case, $\theta = 90^\circ$ and (5) gives the value of 74 Ω. The value obtained from our measurement is 84 Ω. The frequency at which the bow-tie transmission line is one-quarter wavelength

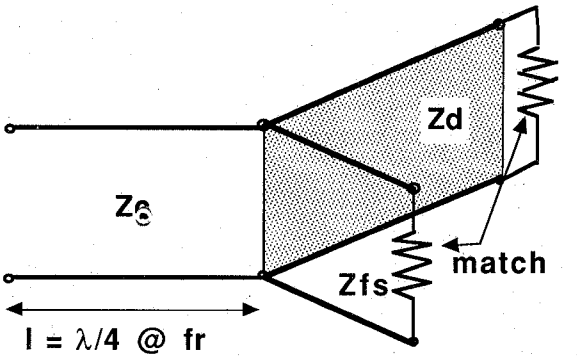

Fig. 10. Transmission line model for the dipole, bow-tie and double-Vee array. Parameters: the dipole array: $Z_c = 166\,\Omega, f_r = 2.524$ GHz; the bow-tie array: $Z_c = 84.4\,\Omega, f_r = 2.55$ GHz; and the double-Vee array: $Z_z - 107.2\,\Omega, f_r = 1.906$ GHz.

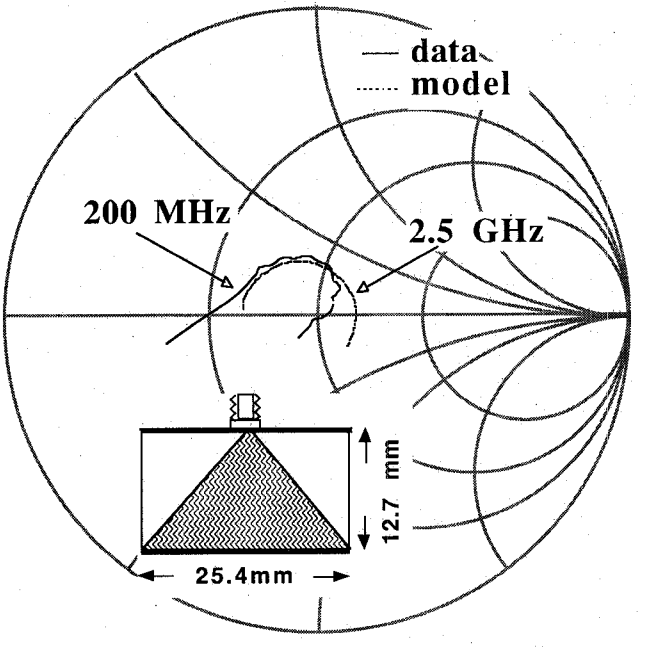

Fig. 11. Bow-tie array results. The Smith chart, normalized to 100 Ω, shows the driving point impedance for the data (solid line) and the equivalent circuit (dashed line) in 130 MHz–3 GHz range. The fit is optimized from 200 MHz to 2.5 GHz. Equivalent circuit is shown in Fig. 10.

long is 2.55 GHz, very close to the corresponding frequency obtained for the dipole transmission line model. The resonance of the bow-tie in an array is at a higher frequency than that of a single bow-tie antenna, which appears to resonate along the edge of the arm [20].

There is a large difference at the very low frequency end between the data and the model. This "low-frequency cutoff" of the measurement method occurs for wavelengths larger than the length of the dielectric transmission line, typically around 200 MHz for our setup. We believe this is an artifact of the measurement method and that the equivalent circuits will describe accurately the 2-D array down to dc.

Double Vee Array

No previous results have been reported on the double-Vee antenna array of Fig. 1(c). However, a double-Vee antenna

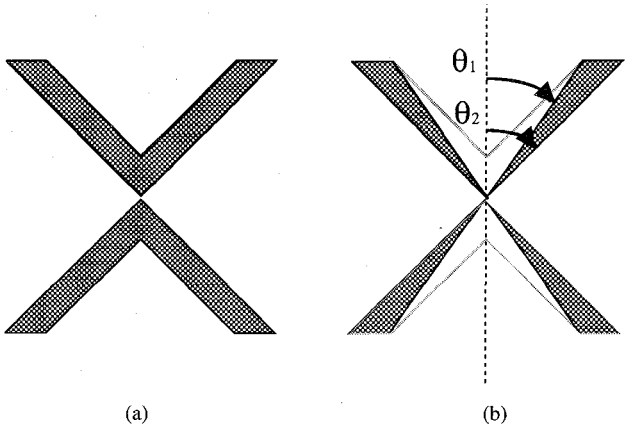

Fig. 12. (a) The double-Vee antenna. (b) The modified double-Vee for which the quasistatic impedance is calculated by the conformal mapping method [22].

can be looked at as a hollowed-out bow-tie antenna. For this reason, we expected the double-Vee array to have a similar equivalent circuit to the bow-tie array.

We can also analyze the double-Vee antenna as a pair of crossed Vee antennas (Fig. 12(a)). With the angle of the Vee of 90° they become the two mutually perpendicular antennas driven from the same point, for which the driving point impedance is one half of that for the single isolated Vee antenna [21]. The modification of the Vee for which the quasistatic impedance is easily obtained by the conformal mapping method is given in [22]. We have used the formula for this modified Vee to calculate the impedance of the double-Vee antenna (Fig. 12(b)):

$$Z_{\text{vee}} = \frac{1}{2}\frac{Z_0}{\sqrt{\frac{1+\epsilon_r}{2}}}\frac{K(k)}{K'(k)}, \qquad k = \frac{\tan\left(\frac{\theta_1}{2}\right)}{\tan\left(\frac{\theta_2}{2}\right)} \tag{6}$$

where $Z_0, \epsilon_r, K(k)$ and $K'(k)$ are the same as for the bow-tie, and θ_1, θ_2 are angles shown in Fig. 12(b). In our case, $\theta_1 = 41.64°$ and $\theta_2 = 45°$ give the value for Z_{vee} of 106.8 Ω.

The results for the double-Vee array are shown in Fig. 13. The equivalent circuit with the best fit is indeed the short transmission line of Fig. 10. The agreement between this simple model and the measured data is obtained in the 200 MHz–1.7 GHz range with less than 0.1% difference. The 107.2 Ω characteristic impedance of the transmission line is in excellent agreement with the calculated value. The frequency at which the Vee transmission line is one-quarter wavelength long (1.906 GHz) is close to f_{ar} calculated (3.b) with l_r the length of an arm of the Vee.

Slot Array

The last array that we present is the slot array (Fig. 1(d)). The simple quasistatic approximation that consists of the series inductance of the short antenna feed and the parallel capacitance of the slot gap was reported to be rather inaccurate [6].

We have obtained an equivalent circuit with excellent fit (0.09% error) to the data in the broader frequency range 200

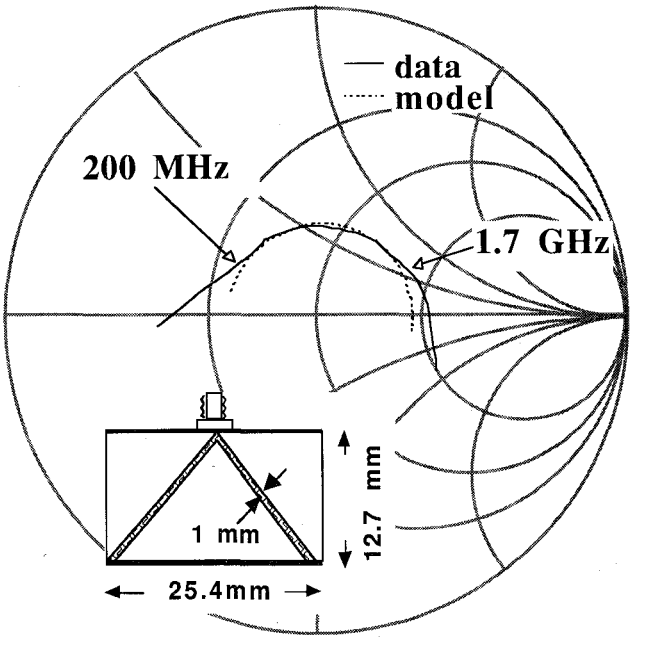

Fig. 13. Double-Vee array results. The driving point impedance for the measured data (full line) and the equivalent circuit (dashed line) are presented on the Smith chart normalized to 100 Ω in the 130 MHz–2 GHz range. Equivalent circuit is shown in Fig. 10.

MHz–3 GHz. The real and imaginary part of the driving point impedance for the measured data (solid line) and our model (dashed line) are shown in Fig. 14(a). The equivalent circuit (Fig. 14(b)) is a simple extension of the L- C quasistatic approximation. It consists of the series inductance $(L1)$ and the series resonant circuit $(L2 - C)$ in parallel with the free space and dielectric transmission lines. The inductance $L1$ can be associated with the short antenna feed, but its value (2.492 nH) is larger than 1.1 nH expected from (4). The inductor $L2 = 2.08$ nH could represent the inductance of the large metal patch of the slot antenna. The capacitance C is the capacitance of the slot gap, but its value (1.05 pF) is much smaller than the 2.32 pF calculated from the quasistatic formula [6]. The resistance $R_s = 284\,\Omega$ has the same meaning as in the dipole model. It is due to radiative losses through the dielectric walls of our model.

Transmission Line Representation

All three of the previously described arrays had simple transmission line models. We show here that the slot array can also be represented by a transmission line model. However, the equivalent circuit obtained (Fig. 14(c)) consists of two transmission lines: TL_1 feeding the middle of TL_2, with the free space and dielectric transmission lines connected at the same point. TL_1 is very short, with $Z_{c1} = 105\,\Omega$ and the one-quarter wavelength frequency f_{r1} of 9.9 GHz. It represents the short antenna feed. We associate TL_2 with the slot; it has Z_{c2} of 163.6 Ω and its total length is one-half wavelength at $f_{r2} = 3.423$ GHz. This value is higher than 2.3 GHz calculated from the mean dielectric constant. TL_2 is open-circuited at its ends, consistent with its termination in a magetic wall. The

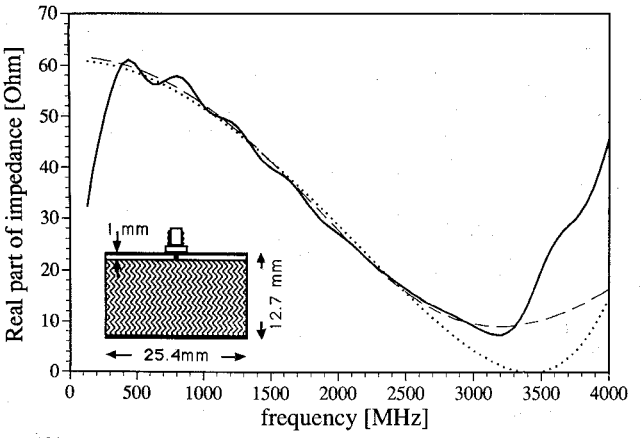

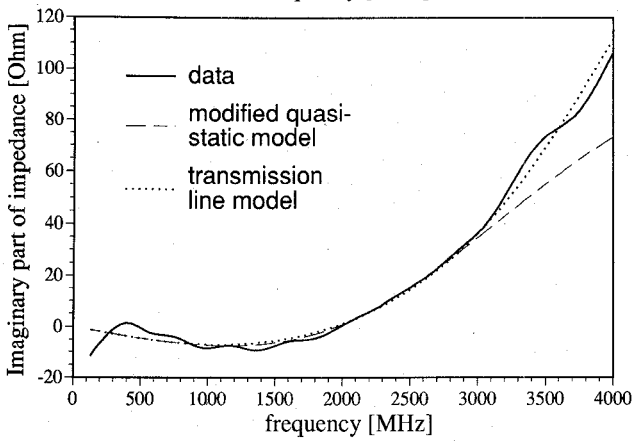

(a)

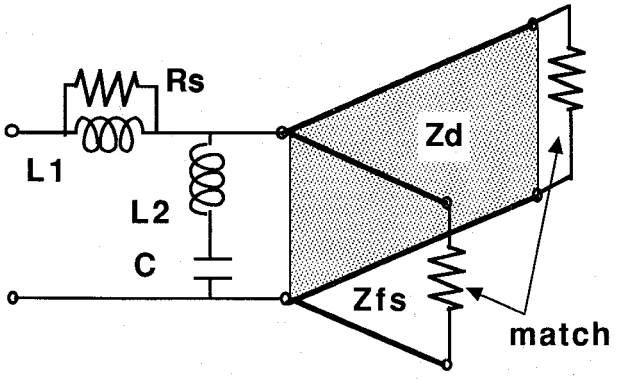

(b)

Fig. 14. Slot array results. (a) Real and imaginary part of the driving point impedance for the measurement (solid line), the improved quasistatic model (dashed line) and the transmission line model (dotted line). (b) Improved quasistatic circuit. *(Continued)*

driving point impedance of this transmission line model is presented in Fig. 14(a) with dotted lines.

Comparison with Theory

We have compared our measurement of slot array with the full-wave rigorous calculations based on the EMF method and presented in [6]. Very good agreement is obtained in both real and imaginary part of impedance in the whole range up to the array resonance (Fig. 15). Note that the calculations were performed for the ideal transmission line, with magnetic walls at the sides. The agreement with theory verifies that the DWM method is a good one for modeling 2-D arrays.

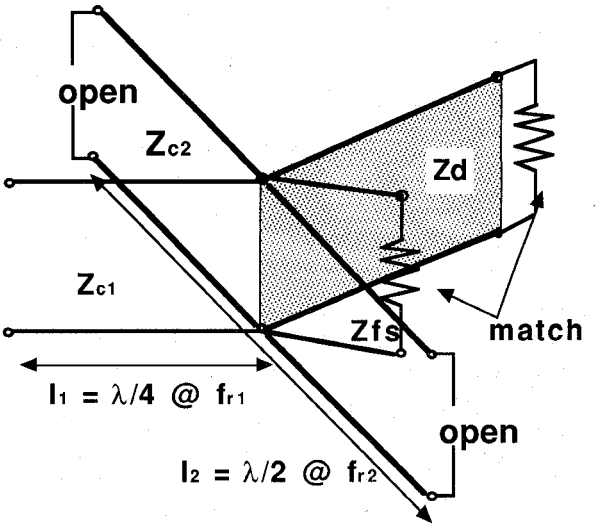

(c)

Fig. 14. *(Continued)* (c) Transmission line model: the transmission line of the short feed ($Z_{c1} = 105\,\Omega$ and $f_{r1} = 9.9$ GHz) connects to the middle of the open-ended slot transmission line ($Z_{c2} = 163.6\,\Omega$ and an electrical length of 180° at $f_{r2} = 3.423$ GHz) in parallel with the free space and dielectric transmission lines.

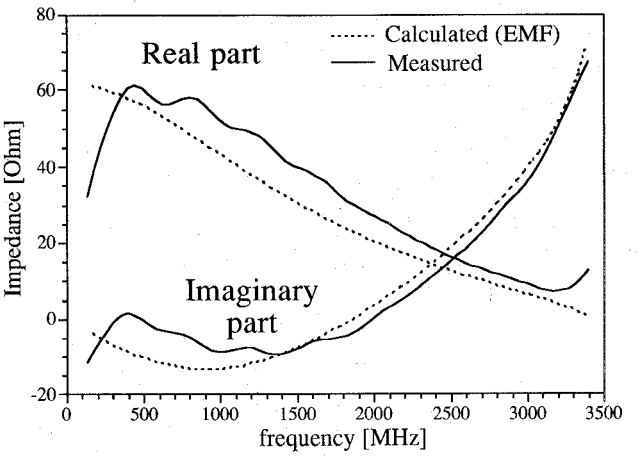

Fig. 15. Real and imaginary part of impedance of the slot array: measured (solid lines) and calculated (dotted lines) [6].

VI. Conclusion

We have demonstrated a simple measurement method for the determination of the driving point impedance of two-dimensional active grid arrays. We have discussed the approximations made to use this method. We have presented the measurements for four antenna arrays of interest. We have obtained simple equivalent circuits that cover the whole baseband operation mode.

We have shown that the results for the dipole and the bow-tie arrays agree very well with the quasistatic predictions and the results reported by others. Our measurements of the slot array agree very well with the full-wave theory in the whole baseband range. This verifies our DWM method. Based on our measurements, we have extended the quasistatic approximation to the double-Vee array with excellent agreement. We have obtained a modified quasistatic circuit for the slot array that fits the measurements very well. Finally, we have shown that

all four antenna arrays can be represented by simple circuits using only transmission lines as circuit elements.

Our results show that of the four arrays, the slot array has the smallest input impedance and the dipole array has the highest. The double-Vee array is a variation of the bow-tie useful where the high inductances of the biasing leads are a requirement. The bow-tie array represents the best combination of the wide baseband operating range and moderate driving point impedance.

The main advantage of the DWM method is its simplicity and ease of use. Driving point impedance of an array is obtained with a one-port measurement over a broad frequency range. The method is applicable to the rectangular arrays of any shape.

REFERENCES

[1] Z. B. Popovic, R. M. Weikle II, M. Kim, and D. B. Rutledge, "A 100-MESFET planar grid oscillator," *IEEE Trans. Microwave Theory Tech.*, vol. 39, pp. 193–200, 1991.

[2] R. A. York and R. C. Compton, "Terahertz Power-combining with Coupled Oscillator Arrays," in *Second Int. Symp. on Space Terahertz Technology*, Pasadena, CA: NASA, 1991.

[3] A. Mortazawi and T. Itoh, "A periodic planar Gunn diode power combining oscillator," *IEEE Trans. Microwave Theory Tech.*, vol. 38, pp. 86–88, 1990.

[4] M. J. Wengler, A. Pance, B. Liu, and R. E. Miller, "Quasioptical Josephson oscillator," *IEEE Trans. Magn.*, vol. 27, pp. 2708–2711, 1991.

[5] B. Liu and M. J. Wengler, "Modeling of quasioptical Josephson oscillator," *IEEE Trans. Applied Superconductivity,* 1991.

[6] D. B. Rutledge and S. E. Schwartz, "Planar multimode detector arrays for infrared and millimeter-wave applications," *IEEE J. Quantum Electron.*, vol. QE-17, pp. 407–414, 1981.

[7] W. W. Lam, C. F. Jou, H. Z. Chen, K. S. Stolt, N. C. Luhman, Jr., and D. B. Rutledge, "Multimeter-wave diode-grid phase shifters," *IEEE Trans. Microwave Theory Tech.*, vol. 36, pp. 902–907, 1988.

[8] D. Kajfez and P. Guillon, Eds., *Dielectric Resonators*. Dedham, MA: Artech House, 1986.

[9] E. A. J. Marcatili, "Dielectric rectangular waveguide and directional coupler for integrated optics," *Bell Syst. Tech. J.*, vol. 48, pp. 2071–2102, Sept. 1969.

[10] H. Kogelnik, "Theory of dielectric waveguides," in *Integrated Optics*, T. Tamir, Ed., New York: Springer-Verlag, 1975, pp. 13–81.

[11] M. Cohn, "Propagation in a dielectric-loaded parallel plane waveguide," *IRE Trans. Microwave Theory Tech.*, vol. MTT-7, pp. 202–208, 1959.

[12] K. C. Gupta, R. Garg, and I. J. Bahl, *Microstrip Lines and Slotlines*. Norwood, MA: Artech House, 1979, pp. 3–6.

[13] H. A. Wheeler, "Transmission-line properties of parallel wide strips by a conformal-mapping approximation," *IEEE Trans. Microwave Theory Tech.*, vol. MTT-12, pp. 280–289, 1964.

[14] {—}{—}, "Transmission-line properties of parallel strips separated by a dielectric sheet," *IEEE Trans. Microwave Theory Tech.*, vol. MTT-13, pp. 172–185, 1965.

[15] *HP8720B Network Analyzer Operating Manual*, Hewlett Packard, 1989.

[16] EESof, Inc., Westlake Village, CA.

[17] R. M. II, Weikle, "Quasi-Optical Planar Grids for Microwave and Millimeter-wave Power-Combining," Ph.D. dissertation, California Institute of Technology, Pasadena, 1991.

[18] R. C. Compton, "Analysis of Millimeter and Microwave Integrated Circuits," Ph.D. dissertation California Institute of Technology, Pasadena, 1987.

[19] D. B. Rutledge, D. P. Neikirk, and D. P. Kasilingam, "Integrated-circuit antennas," in *Infrared and Millimeter Waves*, K. J. Button, Ed. New York: Academic Press, 1983, pp. 1–90.

[20] R. C. Compton, R. C. McPhedran, Z. B. Popovic, G. M. Rebeiz, P. T. Tong, and D. B. Rutledge, "Bow-tie antennas on a dielectric half-space: Theory and experiment," *IEEE Trans. Antennas Propagat.*, vol. AP-35, 1987.

[21] R. W. P. King, *The Theory of Linear Antennas*. Cambridge, MA: Harvard University Press, 1956, pp. 396–397.

[22] D. B. Rutledge, S. E. Schwarz, and A. T. Adams, "Infrared and submillimeter antennas," in *Inf. Phys.*, vol. 18, pp, 713–729, 1978.

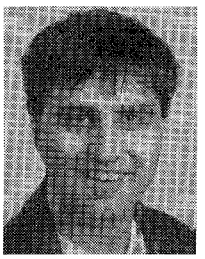

Aleksandar Pance (S'91) was born in Belgrade, Yugoslavia, in 1963. He received the Diplom Engineer degree from the Electrical Engineering Department, University of Belgrade, Yugoslavia in 1987, and the M.S. degree in electrical engineering from the University of Rochester in 1989. He is currently pursuing a Ph.D. degree in electrical engineering at the University of Rochester.

His thesis focuses on Josephson junction oscillators for submillimeter wavelengths. His research interests include high frequency solid-state devices, millimeter-wave and submillimeter-wave active antenna arrays, quasioptical power combining techniques and high speed analog and digital superconducting electronics.

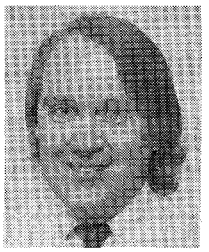

Michael J. Wengler (S'87–M'87) is an Assistant Professor of Electrical Engineering at the University of Rochester. He received his Ph.D. in Applied Physics from the California Institute of Technology in 1987, and his B.A. with honors in Physics from Swarthmore College in 1978. In 1988, he was designated an NSF Presidential Young Investigator.

His primary research area is includes work on quantum measurement theory and the theory and applications of superconducting devices. The superconducting work includes investigation of Josephson junction oscillators and SIS receivers, both for submillimeter wavelengths. His quantum measurement work includes analyses of SIS heterodyne detectors with a quantized radiation field and investigations of the use of SIS heterodyne receivers to detect "squeezed states" of the radiation field. Dr. Wengler is a member of the American Physical Society.

Dr. Wengler is a member of the IEEE Microwave Theory and Techniques Society Speaker's Bureau and the treasurer of the IEEE Electron Devices Society, Rochester Section.